Lab on a Chip

Cite this: *Lab Chip*, 2012, **12**, 1742

www.rsc.org/loc

FOCUS

# Acoustofluidics 11: Affinity specific extraction and sample decomplexing using continuous flow acoustophoresis

**Per Augustsson[a] and Thomas Laurell[ab]**

DOI: 10.1039/c2lc40200a



**Acoustic standing wave technology combined with ligand complexed microbeads offers a means for affinity specific selection of target analytes from complex samples. When realized in a microfluidic format we can capitalize on laminar flow and acoustic forces that can drive cells or microbeads across fluid interfaces. Given this, we have the ability to perform carrier fluid (suspending medium) exchange operations in continuous flow in microfluidic chips based solely on acoustofluidic properties. A key issue here is to ensure that a minimum of the original carrier fluid follows the cells/particles across the fluid interface. Simple processing protocols can be achieved that may outperform macroscale magnetic bead-based sample extraction or centrifugation steps, which can also be straightforwardly integrated with downstream analytical instrumentation. This tutorial outlines some basic fluidic configurations for acoustophoresis based sample decomplexing and details the different system parameters that will impact the outcome of an acoustophoresis based affinity extraction experiment or a cell medium exchange step. Examples are given of both targeted extraction of microbes and selective elusion of molecular species.**

[a]*Department of Measurement Technology and Industrial Electrical Engineering, Division of Nanobiotechnology, Lund University, Sweden. E-mail: per.augustsson@elmat.lth.se; thomas.laurell@elmat. lth.se*
[b]*Department of Biomedical Engineering, Dongguk University, Seoul, Korea*

## 1 Introduction

Affinity specific separations using microbeads in microfluidic systems have emerged as a powerful means of targeted extraction of biological components in crude samples. This has thereafter been a standard in chromatography based systems, with packed microbead columns, for purification or enrichment of molecular species. Extraction of microbial and cellular targets from crude suspensions, however, has had limited success in packed bed based systems. A breakthrough for cell based separation along this line was the introduction of magnetic microbeads/nanoparticles activated with antibodies against cell specific epitopes. In 1977 Molday *et al.*[1] published a seminal paper where anti-mouse immunoglobulin activated magnetic nanoparticles (diameter ≈ 40 nm) bound to B-cells were retained in a magnetic field generated by a horseshoe magnet, while unlabeled cells were washed away. Improved extraction efficiency and process speed was obtained by passing the labeled cell solution through a dense network of ferromagnetic steel wire with the external magnet applied.[2] This provided strong field gradients localized within the wire mesh exerting a retaining force on the labeled cells (Fig. 1). This concept was further developed by Miltenyi *et al.*[3] and was commercialized by Miltenyi Biotech GmbH, providing new methods for affinity specific cell separation in clinical preparatory applications of cell based therapy. More recently, magnetic gradient based microbead manipulation has also gained attention in microfluidic systems after Peyman *et al.*[4] proposed a continuous flow microfluidic chip for rapid surface-based bioanalysis.

## Foreword

In the the eleventh paper of 23 in the *Lab on a Chip* tutorial series of Acoustofluidics, Per Augustsson and Thomas Laurell discuss affinity specific extraction and sample decomplexing using continuous flow acoustophoresis. The basic principle utilized in the tutorial is the ability to perform a medium switch (buffer exchange) of cells and beads using acoustophoresis, a procedure similar to centrifugation and washing but in a continuous format. Different washing devices with labelled and unlabeled cells are outlined as well as important experimental considerations such as diffusion, acoustic streaming, acoustic effects in liquid interfaces and hydrodynamic interactions between particle and fluid.
*Andreas Lenshof – coordinator of the Acoustofluidics series*

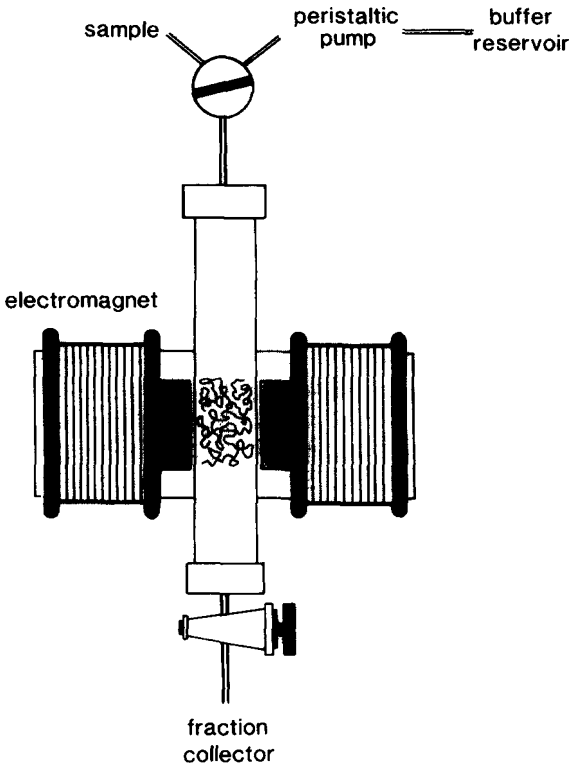


**Fig. 1** Schematic of the original magnetic bead based trapping where locally enhanced magnetic field gradients from a horseshoe magnet was achieved by introducing a ferromagnetic wire mesh in the sample flow. Reprinted from Molday *et al.*[2] with permission from Elsevier.

Analogous to the use of magnetic forces to manipulate magnetic microbeads in complex biological samples, acoustic forces have gained attention as an effective way to control the localization of affinity ligand activated microbeads in microfluidic systems. Acoustic standing wave manipulation of microbeads benefits from flow velocities up to 30 cm $s^{-1}$.[5] The primary acoustic radiation force (PRF) for particles in the 1–10 μm range is substantially higher than the gradient forces reported for magnetic based microsystems.[6,7] The PRF stem from the intrinsic properties of the particles, and therefore acoustophoresis put minimal restriction to the choice of solid phase allowing also for cell based assays.

Target extraction from complex samples using affinity microbead manipulation and acoustic radiation forces in microfluidic systems has been reported in several different modes of operation. Fig. 2(a) shows schematically an acoustophoresis microsystem operated in half wavelength mode where affinity activated microbeads in carrier fluid A containing the sample are translated by the PRF into the pressure node located within the centrally laminated stream of fluid B. The central flow is subsequently collected, holding a purified bead population with the target species bound to the bead surface.[8–11] Fig. 2(b) shows a modified mode of operation where the affinity microbeads are retained in a central pressure node as they move with the carrier fluid A. Along the flow path, a transversal flow of fluid B replaces carrier fluid A while the microbeads are focused to the channel center and

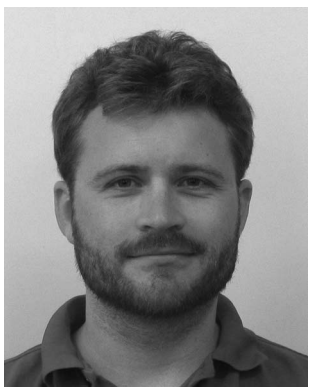

**Per Augustsson**

*Per Augustsson received his M.Sc. degree in engineering physics at Lund University in 2006, and his Ph.D. in 2011. The title of his Ph.D. thesis was "On microchannel acoustophoresis: Experimental considerations and life science applications". His research is focused on acoustofluidic systems for carrier fluid exchange of particles and cells, cell sorting, and measurement systems for assessment of acoustofluidic properties. He has (co)authored 6 peer-reviewed journal papers, as well as 7 peer-reviewed conference contributions.*

**Thomas Laurell**

*Professor Thomas Laurell holds a position as Professor in Medical and Chemical Microsensors and has since 1995 built his research activities around microtechnologies in biomedicine (http://www.elmat.lth.se/forskning/nanobiotechnology_and_labonachip). Laurell recently started a new applied nanoproteomics laboratory at the Biomedical Centre in Lund, integrating microfluidics and nanobiotechnology developments with medical research. This research is focused on new microchip technologies in the areas of biomedicine, biochemistry and nanobiotechnology, with a focus on disease biomarkers, diagnostic microsystems and miniaturised sample processing. Laurell also leads the clinically oriented research environment CellCARE, (www.cellcare.lth.se), which targets chip based cell separation utilising ultrasonic standing wave technology (acoustophoresis) as the fundamental mode of separation.*

a purified bead fraction with target species is obtained at the main outlet.[14] A third mode, Fig. 2(c), of affinity bead operation in microfluidic systems utilizes the possibility to trap beads in a flow channel by generating a local acoustic standing wave field that display a lateral acoustic force potential strong enough to retain the microbeads against the flow. As sufficient numbers of target binding beads have been trapped in the complex fluid A, the input fluid flow is changed to fluid B, whereafter a clean bead suspension with the target species can be released from the trap.[12,13]

The goal of affinity extraction can either be to measure the occurrence of a target species in a sample or to extract a biological target that best matches an affinity ligand from a large population of competitive targets. The latter is commonly performed in the extraction of high affinity binders from engineered molecular libraries of *e.g.* antibodies or aptamers. This may also be practised in situations where efficient extraction of rare species is requested, *e.g.* subspecies of T- or B-cells from blood.

In essence, what constitutes a bio-affinity assay are the following steps:

*i.* mixing of the sample and the affinity ligand activated solid phase (in this tutorial commonly referred to as affinity microbeads)

*ii.* incubation of the sample with the bead affinity mixture

*iii.* carrier fluid exchange/washing, *i.e.* the affinity microbeads are transferred into a fluid free from the complex sample background.

The incubation step is often a rate limiting step controlled by the diffusive and convective conditions of the system as well as the affinity constant, $K_a$, of the affinity ligand to its target, and is often performed off-chip. The washing step is typically repeated several times to accomplish sufficient suppression of the background matrix. The manual procedures often involved in the washing commonly induce loss of the targeted compound after going through several centrifugation and re-suspension steps and hence integration and automation of these steps are desirable, which is why microfluidic implementation can offer attractive alternatives.

This tutorial will describe different microfluidic solutions for affinity bead handling utilizing acoustic standing wave forces. There will be a discussion on considerations that may be valuable to take into account when designing and optimizing an affinity-bead-based acoustofluidic microsystem. The focus will be on continuous flow based affinity acoustophoresis. Acoustic trapping-based bead affinity systems will be described in more detail in the forthcoming tutorials Acoustofluidics 20 (ref. 15) and 21 (ref. 16).

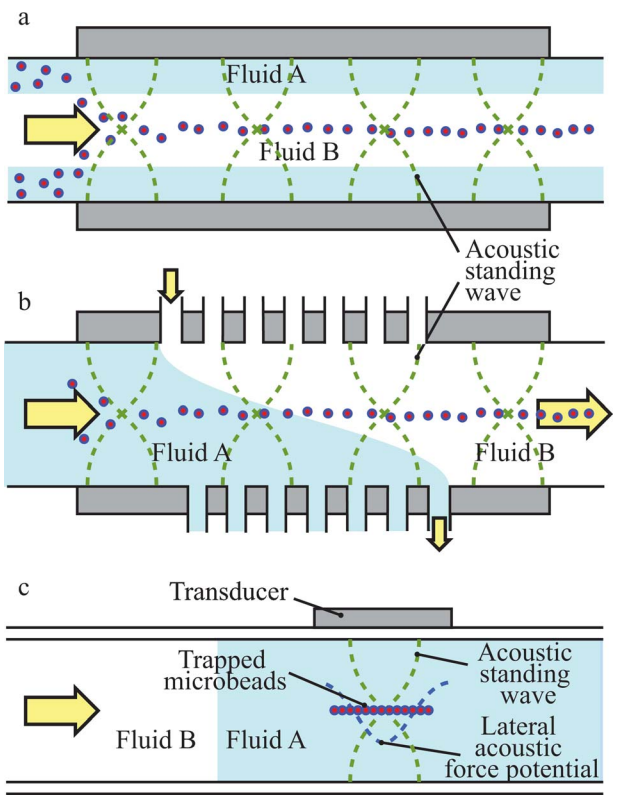


**Fig. 2** Schematic of three different operational modes for acoustic force based extraction of affinity microbeads from a complex sample (A) into a clean fluid (B). (a) Fluids A and B are flow laminated and particles are transferred transverse to the flow by the PRF.[9,11] (b) Particles are retained along the center of a channel by the PRF while fluid A is sequentially exchanged *via* an array of channels branching off on both sides of the main flow.[14] (c) Particles are trapped in a region of the flow by a local acoustic field while the fluid is exchanged.[12,13]

## 2 Theoretical background

### 2.1 Acoustic resonances

A key unit operation in affinity acoustofluidics is the transfer of suspended microbeads or cells by means of acoustic radiation forces. The force potential stems from a local distortion in a resonant sound field due to scattering from the particle, as described in depth in Acoustofluidics 7 (ref. 17). Such 1-, 2- or 3-dimensional resonant acoustic fields can be set up by tailoring of a fluid filled cavity with acoustically hard walls, as presented in Acoustofluidics 5 (ref. 18). From Acoustofluidics 2 (ref. 19), we know that such rectangular cavities can be brought into resonance for frequencies fulfilling

$$f_{n_x,n_y,n_z} = \frac{c_o}{2}\sqrt{\frac{n_x^2}{l^2}+\frac{n_y^2}{w^2}+\frac{n_z^2}{h^2}} \qquad (1)$$

where $l$, $w$, and $h$ are the channel dimensions, $c_o$ is the speed of sound in the fluid and $n_x$, $n_y$, and $n_z$ are the number of half wavelengths along each dimension. In one dimension, *e.g.* if $(n_x, n_y, n_z) = (0, 1, 0)$, eqn (1) reduces to $f = c_o/(2w) = c_o/\lambda$. In experimental reality, if any of the remaining dimensions (here $x$ or $z$) are much longer than the dimension of the primary resonance, a fraction of the acoustic energy will inevitably also resonate along this dimension.

### 2.2 The acoustic radiation force

A particle (a microscopic object such as a microbead, a cell, or a bacterium in a suspension) subjected to a resonant acoustic pressure field, $p_1$, will

 

experience a force, $\boldsymbol{F}_{\mathrm{rad}}$, along the acoustic pressure gradient. In one dimension, the pressure field and the resulting force can be expressed as:

$$p_1 = p_a \cos(k_y y) \tag{2}$$

$$\boldsymbol{F}_{\mathrm{rad}} = 4\pi\, \Phi a^3 k_y E_{\mathrm{ac}} \sin(2k_y y) e_y \tag{3}$$

$$\Phi = \frac{f_1}{3} + \frac{f_2}{2} = \frac{1-\tilde{\kappa}}{3} + \frac{\tilde{\rho}-1}{2\tilde{\rho}+1} \tag{4}$$

$$E_{\mathrm{ac}} = \frac{p_a^2 \kappa_o}{4} \tag{5}$$

where $p_1$ is the first order pressure field of amplitude $p_a$, $y = 0$ at the channel wall (most often the pressure variations are maximal at the walls), $a$ is the particle radius, $k_y = 2\pi/\lambda$ is the wave vector, $E_{\mathrm{ac}}$ is the acoustic energy density, $\Phi$ is the acoustophoretic contrast factor, $\kappa$ is the compressibility of the carrier fluid, and $\tilde{\kappa}$ and $\tilde{\rho}$ are the relative compressibility and density of the particle with respect to the carrier fluid.[17,20] From eqn (4) we see that $\Phi$ increases with relative density and decreases with relative compressibility. Most particles such as polymer beads, cells and other biological objects will move towards the pressure node in the center of the channel, if suspended in *e.g.* water or PBS. For particles lighter and/or more compressible than water, the sign of $\Phi$ becomes negative and the particles move towards the channel walls.

### 2.3 Acoustophoretic velocity

Balancing eqn (3) with the Stokes drag force, we arrive at an approximate expression for the acoustophoretic speed $u_{\mathrm{rad}}$ of a suspended particle.

$$u_{\mathrm{rad}} = \frac{2\Phi}{3\eta} a^2 k y E_{\mathrm{ac}} \sin(2k_y y) \tag{6}$$

Here $\eta$ is the dynamic viscosity. It should be noted that the acoustic radiation force amplitude often displays a variation along more than one direction in a cavity.[21] Such, most often, undesired variations are sometimes observed as periodic perturbations of the focusing pattern of the particles.[22] Along the direction of the flow (here $x$), any effect of the variations in the acoustic field will average out.

When a suspension flows through an acoustic cavity, the particle trajectories will be governed by the acoustic force potential and the pressure-driven Poiseuille flow. The motion along the channel is mainly dictated by the parabolic flow profile, which depends strongly on the particle position in the transverse cross section, while the transverse motion is attributed to the acoustic radiation force (Fig. 3).

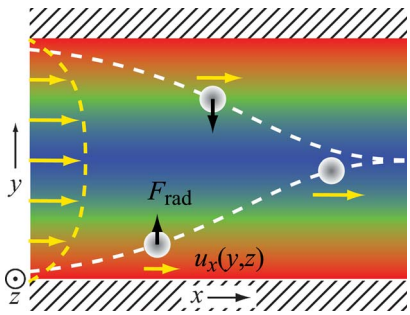


**Fig. 3** Schematic of trajectories for particles flowing through an acoustic radiation force potential. The potential minimum (blue) is aligned along the center of the channel. In all applications covered by this tutorial, the motion $u_x$, along the channel is dominated by the Poiseuille flow profile. Adapted from ref. 23, Lund University, Sweden.

### 2.4 Acoustic streaming

The onset of an acoustic resonance will inevitably induce acoustic streaming in the fluid, which is sometimes referred to as Rayleigh streaming. The theory and applications of acoustic streaming will be covered in depth in upcoming Acoustofluidics tutorials (13 through 16, ref. 24–27). The acoustic streaming emanates from the thin viscous boundary layers at the walls of the acoustic cavity. Inside this thin boundary layer of typical thickness $\delta = 0.5$ μm, oscillatory acoustic energy is converted into a time invariant convective re-circulating flow. Due to the confined geometry, the streaming inside the boundary layer drives a current in the bulk of the fluid, as indicated in the schematic of the channel cross section (Fig. 4). Notably, the direction of the streaming is a function of $y$ and $z$ while the velocity $u_{\mathrm{rad}}$ of a particle ($\Phi > 0$) induced by the acoustic radiation force is always directed towards the central velocity maxima.

Combining the result of Lord Rayleigh for the boundary layer streaming induced by a plane standing wave[28] with eqn (6) yields an approximate relation between the magnitudes of the streaming velocity and the acoustophoretic velocity for a particle.

$$\frac{u_{\mathrm{str}}}{u_{\mathrm{rad}}} = \frac{9\eta}{8\pi\Phi a^2 \rho_o f} = \frac{9\eta\omega}{4\pi\Phi a^2 \rho_o c_o} \tag{7}$$

For a polystyrene particle suspended in a cavity actuated at a resonance frequency of 2 MHz, a critical radius $a_c \approx 1$ μm can be estimated, for which the streaming speed equals the acoustophoretic speed. Notably, for higher frequencies the influence of acoustic streaming diminishes.

Hagsäter *et al.*[29] showed experimentally that the streaming patterns in a straight acoustophoresis microchannel may be far

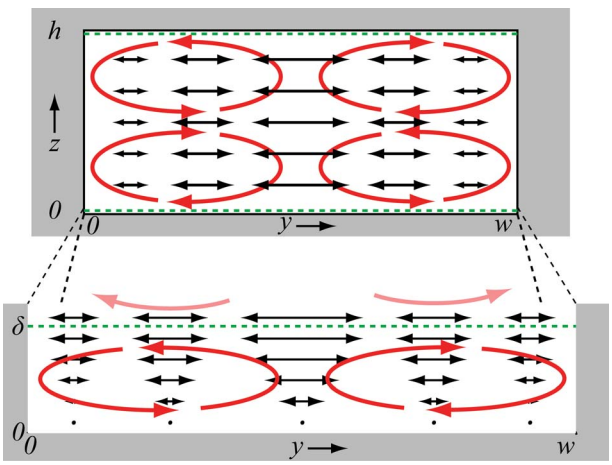


**Fig. 4** Schematic of acoustic streaming in the transverse cross section of an acoustophoresis channel induced by the harmonically oscillating first order acoustic velocity field (black arrows). The lower part shows a close up view of the boundary layer of thickness $\delta$ (green dashed line) and the steady second order streaming velocity field (red arrows). Adapted from ref. 23, Lund University, Sweden.

more complex than the pattern suggested in Fig. 4. Experimental and theoretical quantification of such complex streaming patterns has not yet been satisfactory reported.

## 3 Continuous flow carrier fluid exchange of particles or cells in acoustophoresis microsystems

As already mentioned in the introduction, the ability to transfer particles from one carrier fluid to another is crucial in chip integrated bead-based bio-affinity protocols. Below follow some examples of devices intended for carrier fluid exchange of cells or microbeads. Thereafter, we evaluate some important transport phenomena that ultimately determine the efficiency of these devices.

### 3.1 Devices

Particles can be transferred between two carrier fluids by flow lamination of the original suspension alongside the new fluid and applying a force field perpendicular to the flow direction. The fundamental principle of such a separation strategy, also known as a split-flow thin (SPLITT) separator, was first proposed by Giddings in 1985, using gravitational force to discriminate between large and small particles (Fig. 5(a)).[30] The first implementation of SPLITT fractionation relying on acoustic radiation forces was presented by Johnson *et al.*[31] in 1995 in an mm-scale device intended primarily for particle size discrimination (Fig. 5(b)). The width across this device was 3 mm, corresponding to an acoustic actuator frequency of 250 kHz. The main purpose of the above two devices was to separate particles based on size, but implicitly a carrier fluid exchange was also performed.

The implementation of microscale devices operating in the 1–10 MHz frequency range was a substantial improvement in carrier fluid exchange and size based separation systems since the acoustic focusing rates for microscale systems are considerably faster. For sub MHz systems, acoustic cavitation in the fluid is also more pronounced as the cavitation threshold pressure $p_{cav}$ increases with frequency.

$$p_{cav} \propto f^{1/\alpha} \quad (8)$$

where $\alpha \approx 2$ for water.[33] Cavitation is not desirable since it causes rupture of the cell membranes and mixing of the carrier fluid, which is detrimental in laminar flow

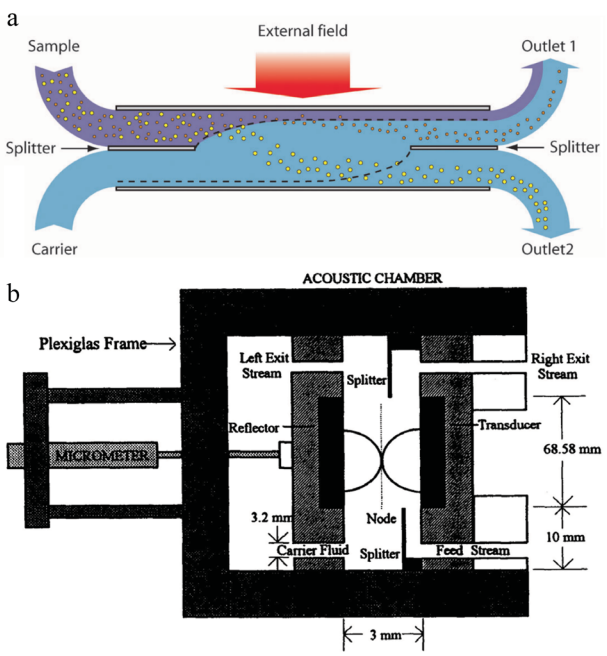


**Fig. 5** (a) Schematic of the thin flow SPLITT fractionator relying on gravitational forces to separate particles of different mass and/or size. Reproduced from Lenshof and Laurell[32] with permission of The Royal Society of Chemistry. (b) The first acoustic continuous flow SPLITT fractionator presented in 1995. Reprinted from by Johnson and Feke[31] with permission from Elsevier.

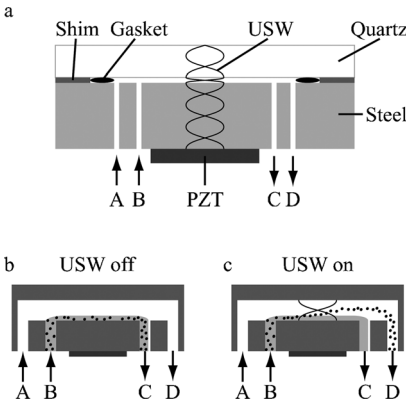


**Fig. 6** (a) Schematic of the device for continuous cell washing presented by Hawkes *et al.*[9] (b) Yeast cells suspended in fluorescein solution was injected through inlet B while yeast and fluorescein free fluid was injected through A. (c) The half wavelength acoustic resonance deflected particles to the mid height of the flow while the original medium remained near the channel floor. At the outlets C and D the flow streams were split and the cells were separated from the fluid containing fluorescein. Reproduced from ref. 9 with permission of The Royal Society of Chemistry.

based separation systems. A higher cavitation threshold allows for higher acoustic energy input and thereby faster acoustic focusing and hence enabling a higher throughput in the device. The cavitation threshold in water extends above 300 kPa, for an ultrasound frequency of 2 MHz, while most experiments are carried out in the range 10 to 100 kPa.

In 2004 Hawkes *et al.*[9] presented a micro-scale acoustic SPLITT-separator for continuous cell washing and mixing. It was demonstrated on a model sample of yeast cells in an aqueous suspension containing dissolved fluorescein dye (Fig. 6(a–c)). In essence, the device is comprised of a flat resonance chamber between parallel plates of quartz and steel, positioned 250 μm apart. Adjusting the actuator frequency to ~3 MHz resulted in a half wavelength resonance across the channel so that cells could be transferred from their initial position near one of the walls at the inlet, to the pressure node centered between the plates. This particular channel was 10 mm wide and the volume flow rate was typically 10 mL $min^{-1}$, which is truly remarkable for a microfluidic system. By expanding the width of the cavity, the volume throughput can be increased

 

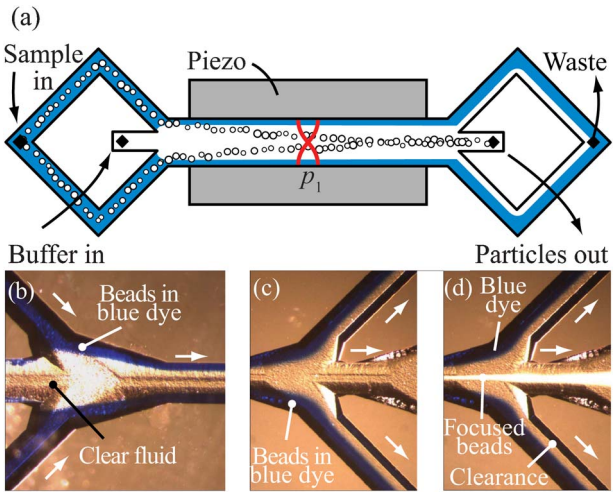


**Fig. 7** The carrier fluid exchange principle introduced by Petersson *et al.*[11] (a) Particles (white) in contaminated carrier fluid (blue) were introduced through a common side inlet. Particles were drawn to the centre of the channel by the acoustophoretic force potential while the blue fluid remained unaffected at the sides. Experimental images of (b) the inlet of the channel, the trifurcation outlet (c) before onset of ultrasound, and (d) during ultrasound actuation. Reproduced from Augustsson *et al.*[8] with permission of Royal Society of Chemistry.

proportionally, while maintaining the same flow velocity and acoustic field amplitude.

In 2005, Petersson *et al.*[11] presented a device for acoustophoretic carrier fluid exchange of blood cells in a silicon/glass microchannel structure (Fig. 7). The proposed areas of applications were blood component washing and bioaffinity assays. A particle suspension was introduced along the side walls of a transverse mode acoustophoresis microchannel while the exchange/wash fluid was infused *via* a central inlet. As the particles flowed along the channel, the acoustic radiation force potential drove them towards the center of the channel, into the stream of exchange fluid. At the end of the channel, the flow was split into a central outlet for the particles in the new carrier fluid, and two side outlets containing the original fluid and particles of low acoustophoretic mobility. The symmetric layout of the inlets and outlets is well suited for half wavelength resonators which have a central acoustic pressure node. While the channel width, $w$, in these systems matches half a wavelength resonance condition, the channel height, $h$, is often kept well below half a wavelength to avoid any secondary resonance component along this direction.

Although high volume throughputs and relatively high recoveries of particulate material were achieved, neither of the above publications report washing efficiencies sufficiently high to be applicable for bioaffinity assays. As we shall see later in this tutorial, this fact may be attributed to cross contamination due to diffusion, acoustically induced streaming, and/or too high particle/cell concentrations.

In 2008, Persson *et al.*[10] used the above mentioned transverse mode acoustophoresis microchannel to select candidates from antibody-displaying bactreriophage libraries (phage display) and thereby outlining a microfluidic based mode of automation of such processes. Microbeads coated with an antigen were incubated with a library of antibody-expressing phages prior to selection. High affinity bacteriophages would thus bind to the microbeads and were separated from low affinity bacteriophages in the chip due to the vast difference in acoustic velocity of the microbeads as compared to the individual phage particles. To achieve sufficient washing efficiency, two serially linked fluid exchange units were incorporated on the same device. Any one out of two antibodies from a small scale model library could be enriched $10^3$ to $10^5$-fold with respect to the other by coating microbeads with the corresponding antigen. From a full library comprising $\sim 10^9$ different antibodies, it was shown that acoustic washing of microbeads yielded antibodies that were indeed specific to the grass pollen allergen Phl p 5 that had been coated on the microbeads. A single run through the device was found to be comparable to 4 manual magnetic bead washing steps, in terms of washing efficiency, for non specific antibodies. The same device was later used for sample decomplexing prior to mass spectrometry readout.[8] A phosphorylated peptide spiked in BSA could be extracted using metal oxide affinity capture beads from the background of highly abundant molecules.

Lenshof *et al.*[34] used an all-glass-fabricated transverse mode acoustophoresis channel for sample preparation of fluorescently labeled cells prior to FACS analysis. Samples of blood were incubated with fluorescently tagged

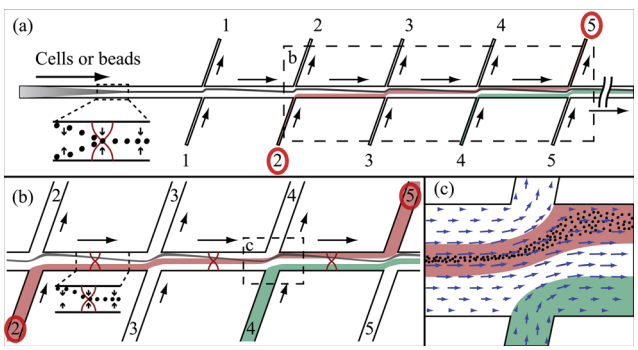


**Fig. 8** The principle of the sequential acoustic carrier fluid exchange channel.[36] (a) Cells or microbeads are initially focused to the center of the flow. The carrier fluid is thereafter exchanged in a number of sequential flow junctions allowing the cells to be exposed to a number of different buffer conditions. (b) If the side channel volume flow rate is set to 1/3 of the main channel flow, a buffer solution infused through *e.g.* side inlet 2 will exit through outlet 5, containing the eluted molecules from the interaction between cells and buffer. (c) At each intersecting flow junction, the particles will follow the fluid flow to the side of the channel and a new buffer will occupy the central part of the channel.

antibodies prior to osmotic RBC-lysis. 60% of the RBC-debris was removed while recovering 99% of the WBC-fraction. The unbound fluorescent dye label was reduced to 1% of the initial concentration.

In 2008, Augustsson *et al.*[14] proposed a method for sequential carrier fluid exchange of cells or microbeads, schematic Fig. 8. The method is similar to that proposed by Yamada *et al.*[35] using hydrodynamic filtration which was demonstrated for studying cell lysis in the millisecond time scale. Particles were initially focused into the center of an acoustophoresis pre-alignment channel, depleting the regions of the flow near the channel walls. At a first intersecting flow junction, a fraction of the main channel flow was extracted on one side of the channel while new carrier fluid was injected on the opposing side. After escaping this flow junction, particles were re-focused into the center of the main channel flow. The process of shifting new medium into the main channel was then repeated in a sequence of consecutive flow junctions. The benefit of this design is the ability to achieve high washing efficiency also for particle rich suspensions. This is possible since the number of sequential shifts can be increased according to the washing requirements. It should be noted that the improved performance comes to the price of an increase in complexity of the fluidic network. An attractive feature of the design is the possibility to perform multiple sequential buffer exchanges,[36] where biological and bioanalytical process steps can be performed in a serial fashion avoiding sample loss and facilitating sample handling. Cell surface bound peptides were extracted in continuous flow by arranging the side channels flow as a sequence of buffers of increasing pH. The pH gradient resulted in a pI related dissociation of peptides and proteins from the cell surface in each buffer stream. The corresponding buffer aliquots were collected and were analyzed using on-line solid phase extraction and MALDI-TOF mass spectrometry.

### 3.2 Experimental considerations

To understand how to design highly efficient devices for carrier fluid exchange of cells and microbeads we will go through some of the fundamental transport mechanisms of suspended and dissolved components, respectively. The fundamental operation in these systems is to transfer particles or cells from their initial suspending fluid near a wall, to a new carrier fluid occupying the central part of the channel, while minute amounts of the original sample fluid, such as antibody-carrying phages, cell debris, dye molecules, or peptides, preferably should remain near the channel walls. Fig. 9 introduces the setting where the particles, which are to be translated into a new carrier fluid (white), enter the system in the sample fluid (gray) along the channel side walls. We recall that $x$, $y$, and $z$ denote positions along the length, width, and height, respectively, $y$ being the axis along which the sound propagates.

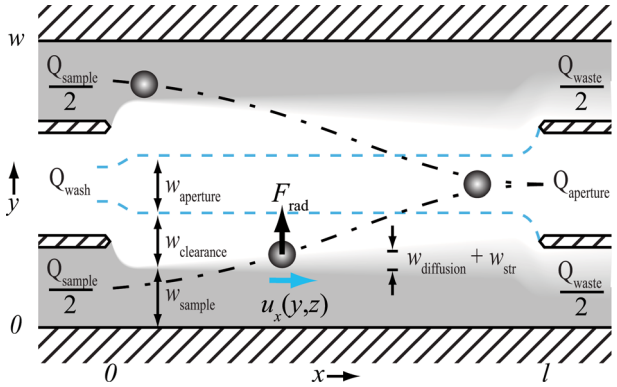


**Fig. 9** Schematic of a generalized acoustophoresis carrier medium exchange channel. Q denotes volume flow rate in the inlets and outlets. Microbeads or cells are focused onto the center of the channel by the force exerted on them through the acoustic resonance. Minute species, *e.g.* non-specific molecular material (gray) remain flow laminated along the channel walls. Each lamina has been assigned a width ($w$), which can be tuned by adjusting the relative volume flow rates (Q) in the inlets and outlets. Adapted from ref. 23, Lund University, Sweden.

**3.2.1 Recovering the particles.** To recover the cells or microbeads in the central outlet while discarding the background, the volume flow rates ($Q$) in the inlets and outlets should be balanced with the acoustophoretic velocity $u_{rad}$. This can be achieved by tuning the acoustic energy density $E_{ac}$ such that the particles reach the channel center before arriving at the outlet trifurcation. Here the center of the channel refers to the part of the flow of width $w_{aperture}$, marked with a blue line in Fig. 9, which is determined by the relative flow rates $Q_{aperture}$ and $Q_{waste}$. According to eqn (6), the transverse velocity $u_{rad}$ of a particle is proportional to the square of its radius $a$, and any minute species of radius $\ll a$ will be efficiently filtered away, regardless of their acoustic properties. We shall see, however, that other effects come into play that may interfere with this statement.

By adjusting the relative flow rates to the inlets, $Q_{sample}$ and $Q_{wash}$, and the outlets, $Q_{aperture}$ and $Q_{waste}$, it is possible to tune the distance $w_{clearance}$ that a particle must travel in order to reach the central outlet. To maximize $w_{clearance}$ the central fluid flow $Q_{wash}$ can be increased relative to $Q_{sample}$ while minimizing the central outlet flow rate $Q_{aperture}$. The washing efficiency and stability of the system can be expected to depend strongly on $w_{clearance}$. Such a clearance will only exist under the condition $Q_{wash}/Q_{sample} > Q_{aperture}/Q_{waste}$. To avoid diluting the central outlet fraction, one can set $Q_{sample} = Q_{aperture}$. Some level of contamination in the central outlet is inevitable and can be attributed to any or one of the following sources:

1. Diffusion of the contaminant
2. Acoustically induced streaming in the lateral cross-section of the flow
3. Non-specific binding of the contaminant to the particles
4. Hydrodynamic interactions between particle and fluid
5. Perturbations in the flow induced by either bubble formation or oscillations in the external fluidics.
6. Mixing of carrier fluids due to destructive radiation pressure in the fluid interface

By quantifying the effect of these phenomena we can estimate the minimum clearance width necessary to maintain high separation efficiency.

 

**3.2.2 Diffusion.** Diffusion of a contaminant from the side inlet to the central outlet can be investigated by comparing the retention time in the device $\tau_{pass} \approx Lwh/Q_{tot}$, to the typical diffusion time $\tau_{diff}$ over the distance $w_{clearance}$. For small ions the diffusion constant $D$ is in the order of $10^{-9}$ m$^2$ s$^{-1}$. *E.g.* for a clearance $w_{clearance} = 100$ μm, the passage time in the device should be less than 1 to 10 s to avoid any notable influence of diffusion. The broadening $w_{diff}$ of the sample stream can be expressed as:

$$\omega_{diff} \approx \sqrt{D\tau_{pass}} = \sqrt{D\frac{L\omega h}{Q_{tot}}} \qquad (9)$$

which verifies that cross contamination due to diffusion is minimized if the flow velocity in the device is high. This can be achieved either by increasing the volume flow rate $Q_{tot}$, or by reducing the channel dimensions. Ref. 9 reports that for the system shown in Fig. 6, diffusion effects were pronounced for fluorescein molecules ($D \approx 5 \times 10^{-10}$ m$^2$ s$^{-1}$). It was suggested that by increasing $w_{clearance}$, the cross contamination due to diffusion could be reduced. This statement can be verified by insertion of the given diffusion coefficient and the channel geometry into eqn (9) which yields the broadening of the sample stream $w_{diff} \approx 20$ μm caused by diffusion. The clearance width in the device was approximately 15 μm, given the flow configuration and the parabolic flow profile. By narrowing the hydrodynamic aperture $w_{aperture}$ by approximately 10% the separation outcome would be dramatically improved. The influence of diffusion is further supported by the higher washing efficiencies reported in ref. 11 (shown in Fig. 7) in which the clearance width was approximately 40 μm, the diffusion rate of the contaminant was also lower, and the flow velocity was higher, yielding a 98% removal of the background (blood plasma) and a recovery of 95% of red blood cells.

**3.2.3 Acoustic streaming.** Lateral acoustic streaming, often referred to as Rayleigh streaming, can convect fluid in the transverse cross section of the channel and thereby transfer minute species to the central outlet. Again taking a look at Fig. 4, we note that for $z = 0$ and $z = h$ the streaming is directed opposite to the acoustophoretic motion of the particles and can therefore not cause transfer of any contaminant to the central outlet. For $z = h/2$, however, the streaming velocity $u_{str}$ coincides with the acoustophoretic velocity of particles $u_{rad}$. During the passage time $\tau_{pass}$ the broadening $w_{str}$ due to streaming can be expressed as:

$$\omega_{str} = u_{str}T_{pass} = u_{str}\frac{\omega/2}{u_{str}+u_{rad}} \approx \frac{\omega/2}{1+\frac{4\Phi\rho_o c_o a^2 k_y}{9\eta}} \qquad (10)$$

where $\tau_{pass}$ is expressed in terms of the time it takes for a particle to traverse the distance $w/2$ under the influence of both the acoustic radiation force and the acoustic streaming. Here we have used eqn (7) to approximate the expression for a given system. Again we remind ourselves that acoustic streaming in microchannel acoustophoresis to a large extent is uncovered ground. Eqn (10) can, however, still yield useful information designing experiments and evaluating operating conditions. For a 5 μm polystyrene bead in aqueous suspension, the maximal streaming broadening is $w_{str} \approx 25$ μm, given an actuator frequency $f = 2$ MHz and that the acoustic energy density $E_{ac}$ is well matched to the flow. For a cell of the same size, more acoustic energy would be required for it to focus in the channel, given its lower acoustic contrast Φ, and consequently $w_{str}$ would increase. Fig. 10(a) is a schematic of the helical motion of two particles caused by acoustic streaming within the bulk fluid of a rectangular shaped microchannel. Fig. 10(b) shows an experimental image of the phenomena, as viewed by confocal microscopy, where a stream of fluorescently tagged lipoproteins enters the system from the side inlets.[37] The image should be viewed as a length wise (along the channel) image slice of the distribution of the fluorophore as it follows the Rayleigh stream while going with the flow.

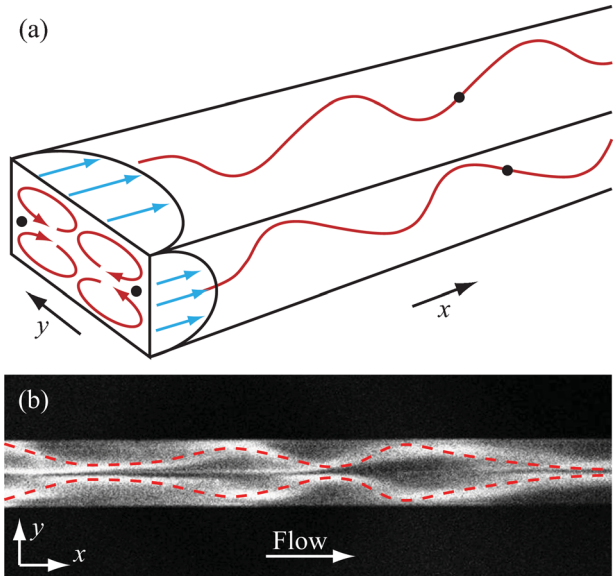


**Fig. 10** (a) Rayleigh streaming in the lateral cross section induces a swirling motion of minute objects as they are convected through the channel. (b) Experimental evidence of fluorescently labeled lipoproteins (VLDL) exhibiting streaming motion in an acoustophoresis channel. The diameter of the vesicles $50 < d < 100$ nm is small enough for acoustic streaming to dominate their motion while being sufficiently large for diffusion to be minimal. Adapted from ref. 37, Lund University, Sweden.

Ref. 11 reports that polyamide microbeads were washed from a dye in a configuration where the system was initially tuned such that particles were focused precisely before the end of the channel. By adjusting the piezo actuator voltage $U_{piezo}$, the acoustic energy was increased 5-fold ($E_{ac} \propto U_{piezo}^2$), resulting in a dramatic increase in contaminant transfer. This suggests that the streaming velocity in the fluid, in the case of the 5-fold acoustic energy, was of the same magnitude as the acoustophoretic bead motion for the first setting. Similarly, in ref. 9, yeast cells were reported to reach their intended outlet already at 25% of the

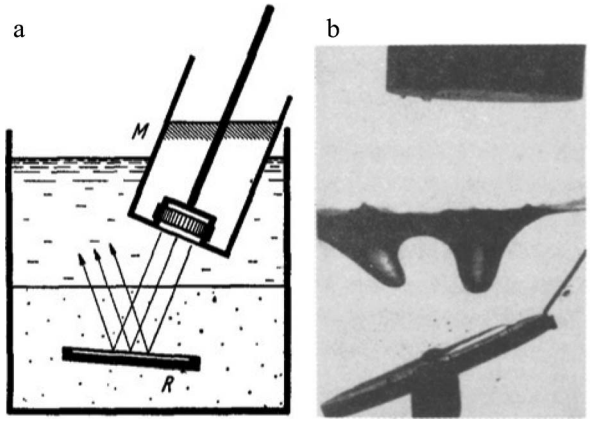


**Fig. 11** (a) Schematic of the experimental set-up of Hertz *et al.*,[38] demonstrating the effect of radiation pressure at the interface between two liquids having different acousto-physical properties (water above and aniline below). (b) The interface curvature of the liquid interface due to an incoming sound beam in water and the beam reflected from the plate submerged in aniline. The acoustic force induced on the interface is dependent of the acoustic energy density in the two media and hence independent of the incident direction of the sound as evidenced by the interface curvature from the reflected sound. Reproduced from ref. 38 with kind permission from Springer Science + Business Media.

energy level required to induce substantial amount of acoustic streaming.

Based on this reasoning, it is recommended that the flow conditions and the actuator power is tuned in regards to the species of interest for each particle wash experiment to suppress carry-over from the original carrier fluid.

**3.2.4 Acoustic radiation pressure in liquid interfaces.** When an acoustic sound beam wave impinges on an interface between fluids of different acoustic properties the interface will deform due to the acoustic radiation pressure (Fig. 11(a and b)).[38] This effect is also present in resonant systems, and Johansson *et al.*[39] demonstrated that it could be used to induce fluid mixing at interfaces. Fig. 12(a–c) shows an experiment where acoustically induced relocation of fluids of different acoustic properties is performed. The effect was present when the acoustic impedance ($Z = \rho c$) of the central fluid was lower than that of the side flows. In acoustophoresis carrier fluid exchange systems this type of acoustic switching may occur where the contaminant fluid relocates to the central position of the flow. Blood cells can, for example, not be straightforwardly extracted directly from undiluted plasma (*i.e.* whole blood) into PBS due to the difference in acoustic properties between the two fluids. The high protein content of blood plasma makes it less compressible and denser than PBS. For a configuration where plasma is flow laminated along each side of PBS, the onset of an acoustic resonance renders an inward pointing acoustic radiation pressure on the interface between the two fluids. Any inhomogeneity in the acoustic field along the channel will cause the delicate balance to collapse and the fluids to relocate. Dilution of the plasma and/or alteration of the central fluid stream are suggested to circumvent the problem.

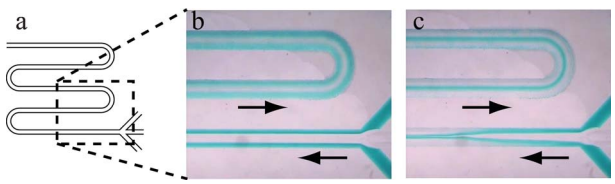


**Fig. 12** Acoustic radiation pressure acting at the interface between two media of different acoustic contrast. (a) Schematic of a trifurcation inlet meandered microchannel. (b) Saline solution spiked with green dye is infused along both sides of MilliQ water. Diffusion is pronounced at the second meander. (c) After the onset of ultrasound, the saline solution is focused to the central part of the flow due to its higher acoustic contrast. Reproduced with kind permission from Carl Grenvall, Lund University, Sweden.

**3.2.5 Non-specific binding.** In the sample inlet, each bead is associated with an average number of non-specific contaminant molecules. The total number of molecules that can potentially be transferred to the central outlet through non-specific binding is therefore proportional to the concentration of beads in the suspension. Ref. 8 reports an evaluation of washing efficiencies for particle concentrations evaluated in the range $5 \times 10^6$ mL$^{-1}$ to $10^9$ mL$^{-1}$. In that range, the contamination per bead was indeed found to be constant. It can be speculated to what extent any weakly adsorbed molecules have time to displace from the surface of a microbead during the passage of $w_{\text{clearance}}$. The number of molecules bound to a surface at a specific time point is related to the concentration of molecules in the fluid and the affinity constant:

$$K_a = \frac{\text{on-rate}}{\text{off-rate}} \qquad (11)$$

which relates the probability for a molecule to remain on the surface to the probability of a molecule to displace. When the surrounding fluid is exchanged, the system is out of equilibrium and molecules of high off-rate will displace from the surface and result in background carry-over.

**3.2.6 Hydrodynamic interactions between particle and fluid.** When a sphere is dragged through a fluid by a force $\boldsymbol{F}_{\text{rad}}$, it will exert that same force on the fluid through friction at the surface (Fig. 13(a)). The overall volume force exerted on the fluid is proportional to the number of suspended particles and increases linearly with the particle radius for a given particle concentration and velocity. This volume force causes convection of the fluid, and when this velocity becomes substantial relative to the velocity of the individual particles, the particles can be considered to be hydrodynamically coupled (Fig. 13(b)). Modeling of such hydrodynamic coupling has been reported by Mikkelsen *et al.*[40] in 2005. Numerical calculations for paramagnetic beads ($a = 0.5$ μm) in a magnetic field yielded that the hydrodynamic

 

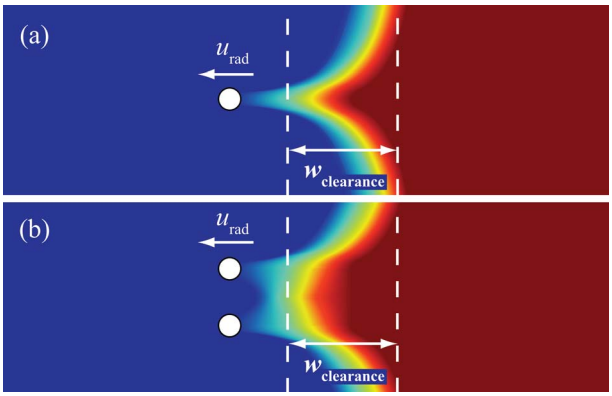


**Fig. 13** (a) Schematic drawing of a sphere moving through an interface between two fluids. The concentration profile of the contaminant (red: high, blue: low) is affected by the drag from the sphere. (b) The combined drag from two closely spaced spheres will convect more contaminant than two largely spaced spheres due to hydrodynamic coupling. Adapted from ref. 23, Lund University, Sweden.

interaction between spheres was minimal for concentrations up to $10^8$ mL$^{-1}$, which corresponds to an average inter particle distance of $d \approx 20$ μm. For higher concentrations the interaction increases exponentially, and at $10^{10}$ mL$^{-1}$ ($d \approx 5$ μm) the particles are fully coupled and drag along all intermediate fluid. Ref. 11 reports a washing experiment with particle concentrations ranging from $5 \times 10^{10}$ mL$^{-1}$ to $2 \times 10^{11}$ mL$^{-1}$, using polyamide beads ($a = 2.5$ μm). From that experiment it is clear that the washing efficiency decreased dramatically for concentrations above $10^{11}$ mL$^{-1}$. Ref. 9 reports a breakdown in washing efficiency at a concentration of yeast cells of $10^8$ mL$^{-1}$. It is reasonable to assume that this type of break down is caused by hydrodynamic coupling between particles.

**3.2.7 Flow perturbations.** Reproducibility and efficiency of the system rely on stable flow conditions. Consider a situation where the flow in the channel is temporarily disrupted by a short plug of air entering the channel inlet and passing through main channel, causing complete mixing of the two inlet streams. Before and after this disturbance the separation is ideal, *i.e.* no contaminant is transferred to the central outlet. The impact of such a perturbation can be estimated from the channel dimensions, and the flow rates in the inlets and outlets. The number of molecules in the channel at complete mixing can be expressed as

$$N_{channel} = \frac{C_{sample} V_{channel} Q_{sample}}{Q_{tot}} \quad (12)$$

The central outlet concentration will be the fraction of those molecules that reach the central outlet sample divided by the final volume of the processed sample.

$$C_{outlet} = \frac{N_{channel} Q_{aperture}}{Q_{tot} V_{outlet}} \quad (13)$$

Insertion of some relevant numbers for a separation setup and a processed volume of 1 mL yield a contamination level of 10 ppm in the central outlet fraction. Ref. 10 and 8 deal with separation of microbeads from non-specific material. In the context of bacteriophage antibody library selections, it can be noted that this level of contamination corresponds to a two times repeated manual washing procedure. This type of disturbance to the flow is one of the main concerns regarding stability and reproducibility in microfluidic cell and bead handling systems in general and washing applications specifically.

**3.2.8 The timing dynamics.** A minimum requirement for continuous flow carrier fluid exchange is that the particles must outrun diffusion, which for the smallest ions implies an acoustophoretic velocity $u_{rad}$ in the order of 100 μm s$^{-1}$. Evander *et al.*[5] report a maximal flow velocity of 25–30 cm s$^{-1}$ while focusing microbeads in a 3 cm long acoustophoresis glass device, which corresponds to an approximate acoustophoretic velocity $u_{rad} \approx 1$–2 mm s$^{-1}$. For continuous flow mode of operation, heat dissipation in the transducer at elevated actuation power is the main limitation regarding particle transition time and implicitly also the volume flow rate. In the experiments the net power delivered to the device was 0.5 W and this did not cause any substantial heating of the device.

For transient onset of sound, transition times of less than 20 ms per 100 μm have been reported[41] and the transition time can probably be further shortened to only a few milliseconds. An ultimate limit is difficult to predict but it can be concluded that transient onset times much shorter than 1 ms are problematic since the high quality factor ($100 < Q < 1000$, ref. 42) in these systems implies a resonance buildup time $\tau = Q/f$ ranging from 0.1 to 1 ms.

**3.2.9 Temperature stability.** The influence of temperature fluctuations in these systems deserves some attention since most of the delivered electric power is dissipated in the assembled actuator/microchip device and converted into heat. Since compressibility and density are temperature dependent parameters, a temperature change will alter the resonance mode in the cavity. According to ref. 21 the frequency shift due to a temperature change was 2 kHz °C$^{-1}$. Since the resonance peak width was measured to be only 8 kHz, a temperature shift of only 1 °C would dramatically affect the acoustic amplitude in the channel. It should be stressed, however, that systems of lower Q-factor, *i.e.* more lossy and/or bulkier, are likely to be less sensitive to temperature fluctuations. For example, Hawkes *et al.*[43] report a frequency shift of 5 kHz °C$^{-1}$ and a corresponding peak width of ~100 kHz. In order to ensure that temperature variations are not affecting the outcome of the acoustofluidic experiment, it is advised to measure the temperature dependency for each platform, or to ensure that the chip temperature is not changing significantly during the experiment. Temperature can be straight forwardly controlled using a Peltier element and a temperature sensor.[21]

## 4 Outlook

Affinity based extraction of components from complex samples is a key unit operation in many analytical, bioanalytical and clinical applications. The most widely used methods today are either centrifugation or magnetic bead

based systems. Affinity acoustophoresis is a relatively new means to accomplish the corresponding result, and it was not until the past few years that the possibility of performing targeted extraction in a continuous flow system has shown promising results. The ability to carry out basic operations in acoustic particle or cell washing clearly demonstrate the benefits of acoustophoresis, especially in systems where a centrifugation step otherwise is the entry point for downstream analysis. A key benefit in this respect is the elimination of manual intervention in the sample handling process, which opens the route to fully integrated analytical systems where a crude sample enters the system and an analytical readout is obtained, *cf.* the above described sample washing prior to FACS analysis. It can also be noted that in comparison to other microfluidic principles of bead handling and affinity extraction, acoustic standing wave based systems generally display a higher throughput, often operating in a range from 100 μL $min^{-1}$ to 10 mL $min^{-1}$. An attractive outlook to acoustic systems is the design of sequential acoustophoresis systems that can perform multiple carrier fluid transfers. We have seen an example of this in the sideways translation of the carrier fluid (Fig. 8). This modality could also be realized in a serial fashion, enabling controlled sequences of ligand interaction, washing, secondary binders *etc.* In such systems it will be of importance to tune flow conditions such that the duration of each step is sufficient, but once in place this would indeed constitute an attractive sample-to-answer system. Crude sample in – data out.

Affinity based particle processing and washing can be performed in other acoustic configurations as well where *e.g.* the particles/cells are retained in an acoustic trap and the background carrier fluid is sequentially replaced by a clean fluid. Acoustically controlled affinity interaction can also be performed at ligand complexed surfaces by adjusting the acoustic standing wave position in proximity with the resonator wall in a microfluidic cell. Both these modalities will be covered in the forthcoming Tutorial issues, Acoustofluidics 20 (ref. 15) and 21 (ref. 16).

## Acknowledgements

Financial support is acknowledged from Swedish Research Council (VR 621-2010-4389), Vinnova Innovationer för Framtidens Hälsa—CellCARE, Formas—TvärLivs—Dnr.: 222- 2010-413, Royal Physiographic Society, Crafoord Foundation.

## References

1 R. S. Molday, S. P. S. Yen and A. Rembaum, *Nature*, 1977, **268**, 437–438.
2 R. S. Molday and L. L. Molday, *FEBS Lett.*, 1984, **170**, 232–238.
3 S. Miltenyi, W. Muller, W. Weichel and A. Radbruch, *Cytometry*, 1990, **11**, 231–238.
4 S. A. Peyman, A. Iles and N. Pamme, *Lab Chip*, 2009, **9**, 3110–3117.
5 M. Evander, A. Lenshof, T. Laurell and J. Nilsson, *Anal. Chem.*, 2008, **80**, 5178–5185.
6 J. Nilsson, M. Evander, B. Hammarstrom and T. Laurell, *Anal. Chim. Acta*, 2009, **649**, 141–157.
7 N. Pamme, *Lab Chip*, 2007, **7**, 1644–1659.
8 P. Augustsson, J. Persson, S. Ekström, M. Ohlin and T. Laurell, *Lab Chip*, 2009, **9**, 810–818.
9 J. J. Hawkes, R. W. Barber, D. R. Emerson and W. T. Coakley, *Lab Chip*, 2004, **4**, 446–452.
10 J. Persson, P. Augustsson, T. Laurell and M. Ohlin, *FEBS J.*, 2008, **275**, 5657–5666.
11 F. Petersson, A. Nilsson, H. Jönsson and T. Laurell, *Anal. Chem.*, 2005, **77**, 1216–1221.
12 M. Evander, K. M. Horsman, C. J. Easley, J. P. Landers, J. Nilsson and T. Laurell, *in 10th International Conference on Miniaturized Systems for Chemistry and Life Sciences*, Tokyo, Japan, 2006.
13 B. Hammarström, J. Nilsson, T. Laurell and S. Ekström, *in The 15th International Conference on Miniaturized Systems for Chemistry and Life Sciences*, Seattle, USA, 2011.
14 P. Augustsson, L. B. Åberg, A.-M. K. Swärd-Nilsson and T. Laurell, *Microchim. Acta*, 2009, **164**, 269–277.
15 M. Evander and J. Nilsson, *Lab Chip*, 2012, Acoustofluidics 20, in press.
16 M. Wiklund, *Lab Chip*, 2012, Acoustofluidics 21, in press.
17 H. Bruus, *Lab Chip*, 2012, **12**, 1014–1021.
18 A. Lenshof, M. Evander, T. Laurell and J. Nilsson, *Lab Chip*, 2012, **12**.
19 H. Bruus, *Lab Chip*, 2012, **12**, 20–28.
20 L. P. Gor'kov, *Sov Phys Doklady*, 1962, **6**, 773–775.
21 P. Augustsson, R. Barnkob, S. T. Wereley, H. Bruus and T. Laurell, *Lab Chip*, 2011, **11**, 4152–4164.
22 R. J. Townsend, M. Hill, N. R. Harris and N. M. White, *Ultrasonics*, 2006, **44**, e467–471.
23 P. Augustsson, *Ph.D. Thesis*, Lund University, 2011.
24 S. S. Sadhal, *Lab Chip*, 2012, Acoustofluidics 13, in press.
25 S. S. Sadhal, *Lab Chip*, 2012, Acoustofluidics 15, in press.
26 S. S. Sadhal, *Lab Chip*, 2012, Acoustofluidics 16, in press.
27 M. Wiklund, R. Green and M. Ohlin, *Lab Chip*, 2012, Acoustofluidics 14, in press.
28 L. Rayleigh, *Philos. Trans. R. Soc. London*, 1884, **175**, 1–21.
29 S. M. Hagsäter, A. Lenshof, P. Skafte-Pedersen, J. P. Kutter, T. Laurell and H. Bruus, *Lab Chip*, 2008, **8**, 1178–1184.
30 J. C. Giddings, *Sep. Sci. Technol.*, 1985, **20**, 749–768.
31 D. A. Johnson and D. L. Feke, *Sep. Technol.*, 1995, **5**, 251–258.
32 A. Lenshof and T. Laurell, *Chem. Soc. Rev.*, 2010, **39**, 1203–1217.
33 R. E. Apfel and C. K. Holland, *Ultrasound Med. Biol.*, 1991, **17**, 179–185.
34 A. Lenshof, B. Warner and T. Laurell, *in Micro Total Analysis Systems* 2010, ed. S. Verpoorte, The Chemical and Biological Microsystems Society, Groningen, Netherlands, 2010.
35 M. Yamada, J. Kobayashi, M. Yamato, M. Seki and T. Okano, *Lab Chip*, 2008, **8**, 772–778.
36 P. Augustsson, T. Laurell and S. Ekström, *in Micro Total Analysis Systems* 2008, San Diego, CA, USA, 2008, 671–673.
37 P. Augustsson, *M.Sc. Thesis*, Lund University, 2006.
38 G. Hertz and H. Mende, *Z. Phys.*, 1939, **114**, 354–367.
39 L. Johansson, S. Johansson, F. Nikolajeff and S. Thorslund, *Lab Chip*, 2009, **9**, 297–304.
40 C. Mikkelsen and H. Bruus, *Lab Chip*, 2005, **5**, 1293–1297.
41 C. Grenvall, M. Carlsson, P. Augustsson, F. Petersson and T. Laurell, *in Micro Total Analysis Systems* 2007, ed. J.-L. Viovy, P. Tabeling, S. Descroix and L. Malaquin, Paris, France, 2007, 1813–1815.
42 R. Barnkob, P. Augustsson, T. Laurell and H. Bruus, *Lab Chip*, 2010, **10**, 563–570.
43 J. J. Hawkes and W. T. Coakley, *Sens. Actuators, B*, 2001, **75**, 213–222.

 